Dyes and Pigments 94 (2012) 150–155

Contents lists available at SciVerse ScienceDirect

Dyes and Pigments

journal homepage: www.elsevier.com/locate/dyepig

Effects of different acceptors in phenothiazine-triphenylamine dyes on the optical, electrochemical, and photovoltaic properties

Zhongquan Wan [a], Chunyang Jia [a,*], Yandong Duan [b], Jiaqiang Zhang [c], Yuan Lin [b,**], Yu Shi [a]

[a] State Key Laboratory of Electronic Thin Films and Integrated Devices, School of Microelectronics and Solid-State Electronics, University of Electronic Science and Technology of China, Chengdu 610054, PR China
[b] CAS Key Laboratory of Photochemistry, Institute of Chemistry, BNLMS, Chinese Academy of Sciences, Beijing 100190, PR China
[c] Beijing Spacecrafts, China Academy of Space Technology, Beijing 100190, PR China

ARTICLE INFO

Article history:
Received 27 August 2011
Received in revised form
25 November 2011
Accepted 23 December 2011
Available online 29 December 2011

Keywords:
Phenothiazine
Acceptor
Cyanoacetic acid
Rhodanine-3-acetic acid
Dye-sensitized solar cells
Photovoltaic property

ABSTRACT

In dye-sensitized solar cells (DSSCs), as the excited electrons from dye molecules are injected to the conduction band of semiconductor film through the acceptor moieties, the acceptor groups have significant influences on the photovoltaic properties of the dyes. In this paper, the effects of different acceptor groups (cyanoacetic acid and rhodanine-3-acetic acid) in two phenothiazine-triphenylamine dyes (**PTZ-1** and **PTZ-2**) on the optical, electrochemical properties and photovoltaic performances were studied. In comparison with **PTZ-2**, the photovoltaic performance of **PTZ-1** is significantly improved by replacing rhodanine-3-acetic acid to cyanoacetic acid. The conversion efficiency of solar cell based on the **PTZ-1** is increased about 110%. The lower efficiency of solar cell based on **PTZ-2** is mainly because the delocalization of the excited state is broken between the 4-oxo-2-thioxothiazolidine ring and the acetic acid, which affects the electron injection from **PTZ-2** to the conduction band of TiO_2.

1. Introduction

In dye-sensitized solar cells (DSSCs), the dye is one of the most important components influencing solar cell performance, because the choice of dye determines the photoresponse of the DSSCs and initiates the primary steps of photon absorption and the subsequent electron transfer process. DSSCs based on the Ruthenium sensitizers have shown very impressive solar-to-electric power conversion efficiencies, reaching 11% under standard AM 1.5G sunlight [1]. However, the large-scale application of ruthenium dyes is limited because of costs and environmental issues. More and more efforts have been dedicated to the development of metal-free organic dyes which exhibit not only higher molar extinction coefficients, but also simple preparation and purification procedures at lower cost.

Generally, metal-free organic dyes possess the evident molecular structure of the donor part and the acceptor part bridged by the conjugated chain. Coumarin [2], merocyanine [3], indoline [4], polyene [5], hemicyanine [6], triphenylamine [7], fluorene [8], carbazole [9] and phenothiazine [10] based-organic dyes have been developed. In metal-free organic dyes, the electron acceptor parts have significant influences on the photovoltaic properties due to the excited electrons from the dye molecules are injected to the semiconductor film through the acceptor parts, and typical acceptor groups are cyanoacetic acid and rhodanine-3-acetic acid. For example, Kim et al. employed cyanoacetic acid as the acceptor on triphenylamine-based dye **TA-St-CA** and attained the overall conversion efficiency of 9.1% [11]. Next, the **TA-DM-CA** dye was obtained by structural modification based on **TA-St-CA**, and attained the overall conversion efficiency of 9.67%, which was the highest value among the metal-free organic dyes so far [7]. Ito et al. used rhodanine-3-acetic acid as the acceptor on indoline-based dye **D149** and attained the overall conversion efficiency of 9.03% [12]. A new indoline dye **D205** was designed by introducing an n-octyl substitute onto the rhodanine ring of **D149** and exhibiting an η value of 9.52%, which is the highest efficiency obtained so far among DSSCs based on indoline-based dye [13].

Based on these studies, we can know that the different acceptors have significant influences on the photovoltaic properties of solar cells based on the dyes. Two phenothiazine-triphenylamine dyes (**PTZ-1** [14] and **PTZ-2** [15]), in which the cyanoacetic acid and rhodanine-3-acetic acid as the different acceptor groups were applied in DSSCs (Scheme 1). Here, we focus on the effects of

* Corresponding author. Tel.: +86 28 83202550; fax: +86 28 83202569.
** Corresponding author. Tel.: +86 10 82615031; fax: +86 10 82617315.
E-mail addresses: cyjia@uestc.edu.cn (C. Jia), linyuan@iccas.ac.cn (Y. Lin).

0143-7208/$ – see front matter © 2012 Elsevier Ltd. All rights reserved.
doi:10.1016/j.dyepig.2011.12.009

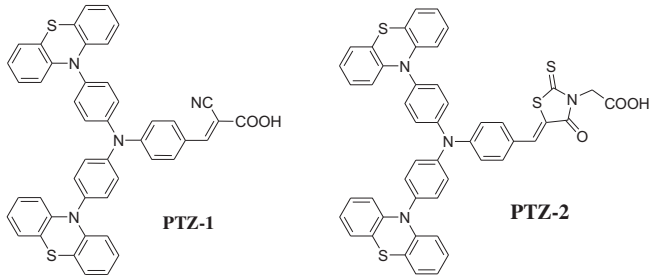

Scheme 1. Molecular structures of **PTZ-1** and **PTZ-2**.

different acceptor groups in **PTZ-1** and **PTZ-2** on the optical, electrochemical properties and photovoltaic performances.

2. Experimental section

2.1. Materials

All solvents and other chemicals were reagent grade and used without further purification. 3-Hexyl-1-methylimidazolium Iodide (HMII) was prepared according to the literature [16]. Lithium iodide (LiI) was purchased from Acros. cyanoacetic acid, rhodanine-3-acetic acid, 4-tert-butylpyridine (TBP) and 3-Methoxypropionitrile (MPN) were purchased from Aldrich.

2.2. Photophysical and electrochemical measurements

Absorption spectra were measured with SHIMADZU (model UV1700) UV–vis spectrophotometer. Emission spectra were recorded with a Hitachi (model RF-5301) Spectrophotometer. Cyclic voltammetry experiments were performed on a CH Instruments 660C electrochemical workstation at a scan rate of 100 mV/s in dimethylformamide (DMF) (5×10^{-4} mol/L) containing 0.1 mol/L n-Bu_4NPF_6 as the supporting electrolyte, platinum as counter and working electrodes and Ag/AgCl as reference electrode.

2.3. Theoretical calculations

Gaussian 03 package was used for Density functional theory (DFT) calculations [17]. The geometries and energies of **PTZ-1** and **PTZ-2** were determined using the B3LYP method with the 6-31G(d,p) basis set. Importantly, none of the frequency calculations generated negative frequencies, being consistent with an energy minimum for the optimized geometry.

Table 1
UV–vis, emission and electronchemical data.

Dye	λ_{max}[a]/nm (ε[b]/M^{-1} cm^{-1})	λ_{ex}[a]/nm	E_{ox}[c]/V (vsNHE)	E_{0-0}[d]/eV	E_{ox}^*[e]/V (vsNHE)
PTZ-1	433 (51,500)	530	0.636	2.626	−1.990
PTZ-2	468 (25,250)	543	0.410	2.476	−2.066

[a] Absorption and emission spectra were measured in CH_2Cl_2 solutions (2.5×10^{-5} M) at room temperature.
[b] The molar extinction coefficient at λ_{max} of the absorption spectra.
[c] The first oxidation potential of the dye was measured in DMF with 0.1 M n-Bu_4NPF_6 as electrolyte (scanning rate: 100 mV s^{-1}, working electrode and counter electrode: Pt wires, and reference electrode: Ag/AgCl), potentials measured vs Ag/AgCl were converted to normal hydrogen electrode (NHE) by addition of +0.2 V.
[d] 0–0 transition energy, estimated from the intercept between absorption and emission spectra in CH_2Cl_2.
[e] The estimated excited state oxidation potential of the dye was calculated from $E_{ox}-E_{0-0}$.

2.4. Fabrication of DSSCs

TiO_2 colloid was prepared according to the literature [18]. The FTO glass substrates were immersed in 4.0×10^{-2} mol/L $TiCl_4$ aq. at 70 °C for 30 min and washed with water and ethanol. The 12 μm thick mesoporous nano-TiO_2 films composed of 15–20 nm anatase TiO_2 particles were coated on the FTO glass plates by doctor blade. After drying the nanocrystalline TiO_2 layer at 125 °C, a 4 μm thick second layer of 300–500 nm sized light scattering anatase particles (Shanghai Cai Yu Nano Technology Co., Ltd, http://shkangyu.cn.gongchang.com) was deposited by doctor blade onto the first layer. The TiO_2 electrodes were heated at 450 °C for 30 min. After the sintering, when the temperature cooled to about 90 °C, the electrodes were immersed in a dye bath containing 2.0×10^{-4} mol/L **PTZ-1** and **PTZ-2** in acetonitrile and left overnight. The films were then rinsed in ethanol to remove excess dye. Solar cells were assembled, using a 25 μm thick thermoplastic Surlyn frame, with a platinized counter electrode. An electrolyte solution was then introduced through the hole predrilled in the counter electrode, and the cell was sealed with thermoplastic Surlyn covers and a glass coverslip. The electrolyte employed was a solution of 0.3 M HMII, 0.5 M LiI, 0.05 M I_2 and 0.5 M TBP in MPN.

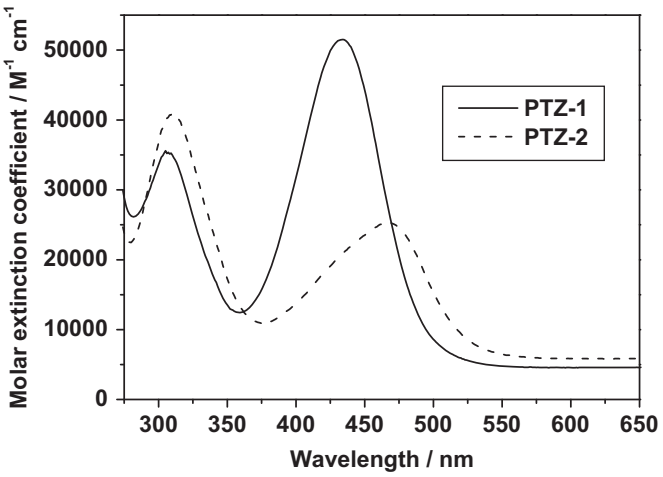

Fig. 1. Absorption spectra of **PTZ-1** and **PTZ-2** recorded in dichloromethane.

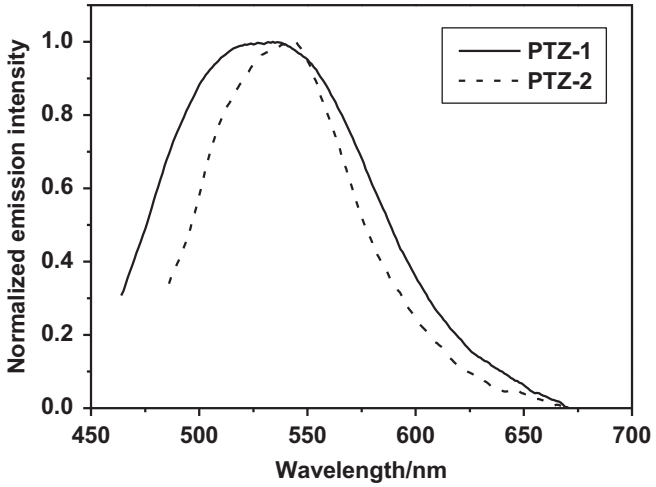

Fig. 2. Emission spectra of **PTZ-1** and **PTZ-2** in dichloromethane.

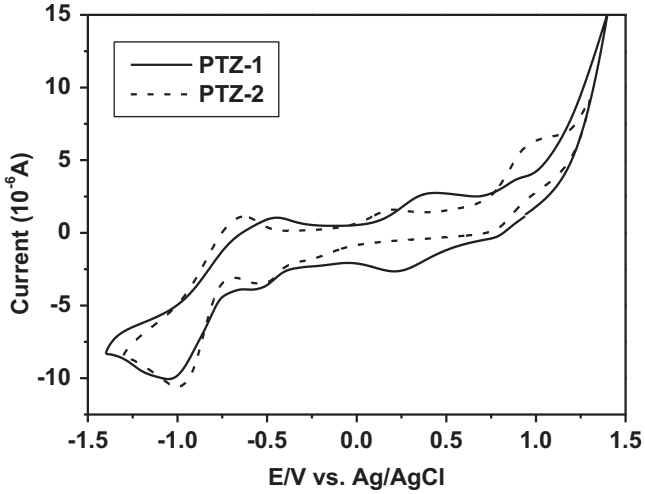

Fig. 3. Cyclic voltammograms of **PTZ-1** and **PTZ-2** in DMF.

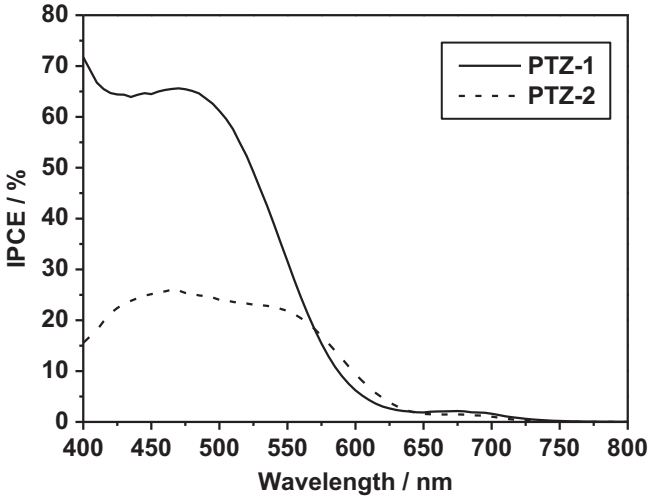

Fig. 5. The IPCE spectra of DSSCs based on **PTZ-1** and **PTZ-2**.

2.5. Photovoltaic characterization

The irradiation source for the photocurrent density–voltage (*J–V*) measurement is an AM 1.5 solar simulator (91160A, Newport Co., USA). The incident light intensity was 100 mW cm^{-2} calibrated with a standard Si solar cell. The tested solar cells were masked to a working area of 0.2 cm^2. Volt-current characteristic were performed on a Model 2611 Source meter (Keithley Instruments, Inc., USA). A Keithley 2611 source meter and a Model spectrapro 300i monochromator (Acton research, USA) equipped with a 500 W xenon lamp (Aosiyuan Technology & Science Co., Ltd, China) were used for photocurrent action spectrum measurements.

3. Results and discussion

3.1. Optical properties

In general, dye is a pivotal and unique component with a function of light-harvesting in DSSCs. Its spectral response overlapped with the solar spectrum will affect the device photocurrent to a large extent. Therefore, we first measured the absorption spectra of the two dyes to have a preliminary evaluation on their light-harvesting capacities.

Fig. 1 shows the absorption spectra of the dyes in dichloromethane, and the corresponding data were summarized in Table 1. With the same donor group, the shapes of the absorption spectra around 305 nm of **PTZ-1** and **PTZ-2** are quite similar, which can be assigned to a $\pi-\pi^*$ transition. The absorption spectrum of the **PTZ-1** has one intense visible absorption band centered at 433 nm (λ_{max}) with molar extinction coefficient (ε) of 51,500 M^{-1} cm^{-1}, which could be ascribed to an efficient intramolecular charge transfer (ICT) between the donor and acceptor groups. On the other hand, **PTZ-2** exhibits an absorption λ_{max} at 468 nm (ε = 25,250 M^{-1} cm^{-1}). The absorption band of **PTZ-2** with rhodanine-3-acetic acid as acceptor exhibits red shift about 35 nm compared to that of **PTZ-1** with cyanoacetic acid as acceptor. This shift is owing to that the rhodanine-3-acetic acid extends the π-conjugation system of **PTZ-2** through the 4-oxo-2-thioxothiazolidine ring. In comparison with **PTZ-2**, the molar extinction coefficient of **PTZ-1** is higher, which is an advantageous spectral property for light-harvesting of the solar spectrum.

Furthermore, the emission spectra of **PTZ-1** and **PTZ-2** were measured in dichloromethane and the corresponding emission maxima located at 530 and 543 nm, respectively, as excited on their absorption maxima (Fig. 2). Based on the intersection of absorption

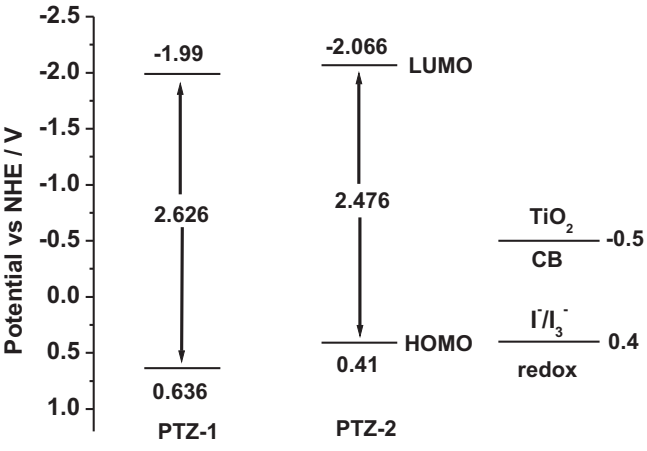

Fig. 4. Schematic energy levels of **PTZ-1** and **PTZ-2** based on absorption and electrochemical data.

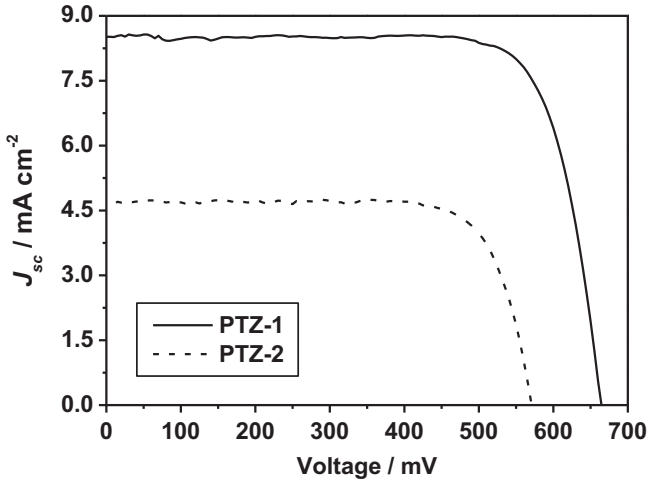

Fig. 6. Current density–voltage curves of DSSCs based on **PTZ-1** and **PTZ-2**.

Table 2
Photovoltaic performance of DSSCs based on **PTZ-1** and **PTZ-2**.

Dye	J_{sc}/mA cm^{-2}	V_{oc}/mV	ff	η/%
PTZ-1	8.5	660	0.79	4.4
PTZ-2	4.7	570	0.78	2.1
N3	17.2	650	0.71	7.9

and emission spectra, the zeroth–zeroth transition energies (E_{0-0}) of **PTZ-1** and **PTZ-2** are estimated to be 2.626 and 2.476 eV, respectively.

3.2. Electrochemical properties

The energetic alignment of the HOMO and LUMO energy levels is crucial for an efficient operation of the dye in DSSCs. To ensure efficient electron injection from the excited dye into the conduction band of TiO_2, the LUMO level must be higher in energy than the TiO_2 conduction band edge. The HOMO level of the dye must be lower in energy than the redox potential of the I^-/I_3^- redox couple for efficient regeneration of the dye cation after photoinduced electron injection into the TiO_2 film. To judge the possibility of electron transfer from the excited dye to the conductive band of TiO_2, cyclic voltammetry were performed to determine redox potentials of the two dyes.

As shown in Fig. 3 and Table 1, the first oxidation potentials (E_{ox}) correspond to the HOMO levels of the dyes (**PTZ-1**: 0.636 V vs NHE; **PTZ-2**: 0.410 V vs NHE) are more positive than the I^-/I_3^- redox potential (0.4 V vs NHE), indicating that the oxidized dyes formed from respective electrons injection into the conduction band of TiO_2 will favorably accept electrons from I^- ions in thermodynamic property. On the other hand, the excited state oxidation potentials (E_{ox^*}) correspond to the LUMO levels of the dyes were calculated from the first oxidation potentials and the E_{0-0} determined from the intersection of absorption and emission spectra. The E_{ox^*} of the dyes (**PTZ-1**: −1.99 V vs NHE; **PTZ-2**: −2.066 V vs NHE) are far more negative than the band edge energy of the nanocrystalline TiO_2 electrode (−0.5 V vs NHE) [19], indicating that the electron injection process from the excited dye molecule to conduction band of TiO_2 is energetically permitted. Therefore, the two dyes will have sufficient driving force for electron transfer from the excited dye molecules to the conduction band of TiO_2.

From these results, we can find the different acceptor groups show a great effect on the HOMO levels and a gentle effect on the LUMO levels. The comparatively lower HOMO level of **PTZ-1** could show a positive effect on DSSCs performance due to the broader gap between the HOMO level and the redox potential of I^-/I_3^- leading to the larger driving force for the reduction of the oxidized dye. The schematic energy levels of **PTZ-1** and **PTZ-2** based on absorption and electrochemical data are shown in Fig. 4.

3.3. Photovoltaic properties

The incident photon-to-current conversion efficiencies (IPCE) of DSSCs based on **PTZ-1** and **PTZ-2** were measured in the visible region (400–800 nm), as shown in Fig. 5. It can clearly be seen that the photocurrent response of **PTZ-1** sensitized DSSCs is much better than that of **PTZ-2** in the range of 400–570 nm. But the photocurrent response of **PTZ-2** sensitized DSSCs is slightly better than that of **PTZ-1** in the range of 570–640 nm. The highest IPCE value of 66% at 470 nm for **PTZ-1** and 26% at 465 nm for **PTZ-2**, respectively. The higher IPCE value of **PTZ-1** in the range of 400–570 nm might attribute to the higher molar extinction coefficient. On the other hand, the photocurrent response of **PTZ-2** sensitized DSSCs is slightly better than that of **PTZ-1** in the range of 570–640 nm might due to the absorption red shift. In comparison with **PTZ-2**, **PTZ-1** gives the higher IPCE value, which implies the dye would show a relatively large photocurrent in DSSCs.

Fig. 6 shows the *J–V* curves of DSSCs based on **PTZ-1** and **PTZ-2** dyes, and the corresponding data are summarized in Table 2 in comparison with that of dye **N3**. Consistent with the result of IPCE, the photovoltaic data show the order of **PTZ-1** > **PTZ-2**. For the more efficient dye, **PTZ-1**, an overall conversion efficiency of 4.4% was obtained with J_{sc} = 8.5 mA cm^{-2}, V_{oc} = 660 mV, and ff = 0.79. Under the same conditions, the **PTZ-2** sensitized cell gave a J_{sc} of 4.7 mA cm^{-2}, an V_{oc} of 570 mV, and a ff of 0.78, corresponding to an overall conversion efficiency of 2.1%. The conversion efficiency of solar cell based on the **PTZ-1** is increased about 110%. These values were comparable to those of the cell based on **N3** (J_{sc} = 17.2 mA cm^{-2}, V_{oc} = 650 mV, ff = 0.71, and η = 7.9%) measured in the same conditions.

According to Figs. 5 and 6, it is clear that the photovoltaic performances of the DSSCs can be evidently affected by the different acceptor groups in the phenothiazine-triphenylamine dyes. In comparison with **PTZ-2**, the photovoltaic performances of **PTZ-1** are significantly improved by replacing rhodanine-3-acetic acid to cyanoacetic acid. The higher IPCE of **PTZ-1** likely results in a higher J_{sc} value compared with that of **PTZ-2**. The higher V_{oc} of **PTZ-1** than that of **PTZ-2** might be due to the comparatively lower HOMO of the former (estimated from the CV), which offers

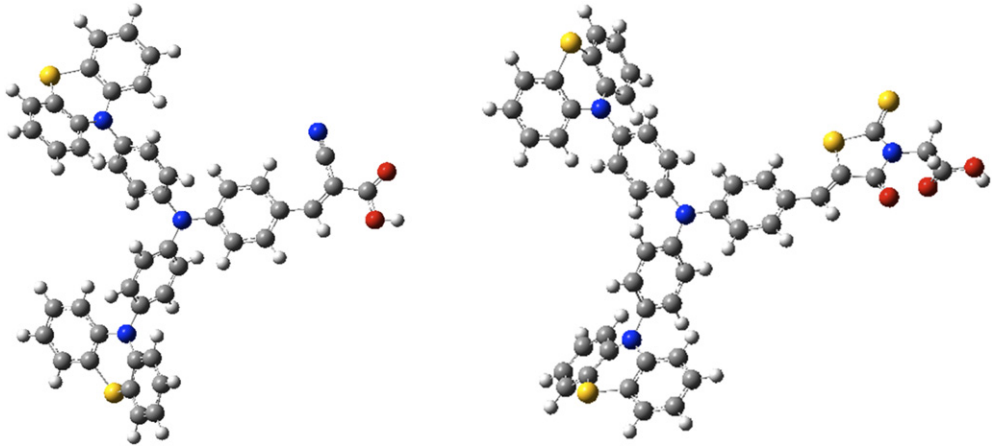

Fig. 7. Optimized geometries of **PTZ-1** (left) and **PTZ-2** (right).

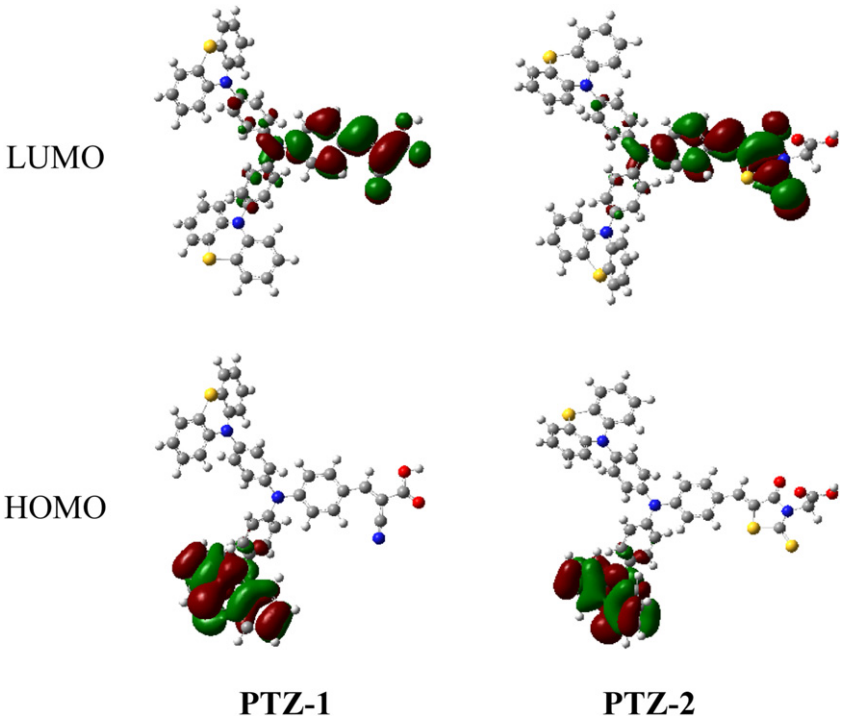

Fig. 8. The electron distribution of the HOMO and LUMO of **PTZ-1** and **PTZ-2**.

larger driving force for the reduction of the oxidized dye. This, in turn, will lead to a slower back electron transfer from TiO_2 to the oxidized dye and result in a lager V_{oc} value [20]. The higher J_{sc} and V_{oc} for the device of **PTZ-1** lead to the higher efficiency finally.

3.4. Theoretical calculations

To get further insight into the effect of molecular structures and electron distributions of **PTZ-1** and **PTZ-2** on the performances of DSSCs, their geometries and energies were optimized by density functional theory (DFT) calculations at the B3LYP/6-31G(d, p) level with Gaussian 03 [17].

From the optimized geometries of the dyes (Fig. 7), we can know that all dihedral angles between phenothiazine and benzene are all noncoplanar, which can help to inhibit the close π−π aggregation effectively between the starburst structures. The noncoplanar configuration can also reduce contact between molecules and enhance their thermo-stability [21].

Fig. 8 shows the electron distributions of the HOMO and LUMO of **PTZ-1** and **PTZ-2**. At the ground state (HOMO) for the two dyes, electrons are homogeneously distributed on phenothiazine ring. The electron density of LUMO of **PTZ-1** is mainly localized on the bridge and anchoring group (−COOH). Therefore, when **PTZ-1** is anchored to TiO_2, the LUMO centered on the anchoring moiety should enhance the orbital overlap with the titanium 3d orbital and subsequently favor the electron injection to the conduction band of TiO_2. On the other hand, the LUMO of **PTZ-2** is mainly centered on the rhodanine, especially on the carbonyl and thiocarbonyl groups, and resulting in the position of LUMO isolated from the −COOH anchoring group due to the presence of $-CH_2$-group. Consequently, **PTZ-2** prevents electrons from being effectively injected into conduction band of TiO_2 *via* the carboxyl group [22]. Obviously, the stronger electron-localization ability of rhodanine-3-acetic acid is resulted from the breaking of the conjugation introduced by the methylene in the rhodanine-3-acetic acid. In comparison with **PTZ-2**, **PTZ-1** can give effective and faster electron injection from the LUMO to conduction band of TiO_2 and reduce the dye recombination, so the solar cell based on **PTZ-1** shows the better photovoltaic performance.

4. Conclusions

In summary, the effects of different acceptor groups in phenothiazine-triphenylamine dyes on the optical, electrochemical, and photovoltaic properties were studied. By replacing the cyanoacetic acid to rhodanine-3-acetic acid as electron acceptor, the absorption spectrum of **PTZ-2** shows a significant red shift due to the rhodanine-3-acetic acid extends the π-conjugation system. The different acceptor groups in **PTZ-1** and **PTZ-2** show a great effect on the HOMO levels and a gentle effect on the LUMO levels. The overall conversion efficiencies of 4.4% and 2.1% were obtained for DSSCs based on **PTZ-1** and **PTZ-2**, respectively. In comparison with **PTZ-2**, the photovoltaic performance of **PTZ-1** was significantly improved by replacing rhodanine-3-acetic acid to cyanoacetic acid. The conversion efficiency of solar cell based on the **PTZ-1** is increased about 110%. Theoretical calculations show that the delocalization of the excited state is broken between the 4-oxo-2-thioxothiazolidine ring and the acetic acid, which affects the electron injection from **PTZ-2** to the conduction band of TiO_2. The results indicate that cyanoacetic acid acceptor favors better properties of DSSCs than that of rhodanine-3-acetic acid acceptor in the phenothiazine-triphenylamine dyes. Further structural optimization, such as broadening the absorption spectra and tuning the energy levels, is very likely to generate more efficient sensitizers and this work is currently underway in our laboratory.

Acknowledgments

We thank the National Natural Science Foundation of China (Grant No. 20602005, 20873015), the Fundamental Research Funds

for the Central Universities (Grant No. ZYGX2010J035), the Innovation Funds of State key Laboratory of Electronic Thin Films and Integrated Device (Grant No. CXJJ201104) and Beijing National Laboratory for Molecular Sciences (BNLMS) for financial support.

References

[1] Chen CY, Wang M, Li JY, Pootrakulchote N, Alibabaei L, Decoppet JD, et al. Highly efficient light-harvesting ruthenium sensitizer for thin-film dye-sensitized solar cells. ACS Nano 2009;3:3103–9.
[2] Seo KD, Song HM, Lee MJ, Pastore M, Anselmi C, Angelis FD, et al. Coumarin dyes containing low-band-gap chromophores for dye-sensitised solar cells. Dyes Pigm 2011;90:304–10.
[3] Ono T, Yamaguchi T, Arakawa H. Study on dye-sensitized solar cell using novel infrared dye. Sol Energy Mater Sol Cells 2009;93:831–5.
[4] (a) Matsui M, Kotani M, Kubota Y, Funabiki K, Jin JY, Yoshida T, et al. Comparison of performance between benzoindoline and indoline dyes in zinc oxide dye-sensitized solar cell. Dyes Pigm 2011;91:145–52;
(b) Dentani T, Kubota Y, Funabiki K, Jin JY, Yoshida T, Matsui M, et al. Novel thiophene-conjugated indoline dyes for zinc oxide solar cells. New J Chem 2009;33:93–101;
(c) Matsui M, Fujita T, Kubota Y, Funabiki K, Jin JY, Yoshida T, et al. Substituent effects in a double rhodanine indoline dye on performance of zinc oxide dye-sensitized solar cell. Dyes Pigm 2010;86:143–8.
[5] Hara K, Sato T, Katoh R, Furube A, Yoshihara T, Murai M, et al. Novel conjugated organic dyes for efficient dye-sensitized solar cells. Adv Funct Mater 2005;15:246–52.
[6] Chen YS, Li C, Zeng ZH, Wang WB, Wang XS, Zhang BW. Efficient electron injection due to a special adsorbing group's combination of carboxyl and hydroxyl: dye-sensitized solar cells based on new hemicyanine dyes. J Mater Chem 2005;15:1654–61.
[7] Im H, Kim S, Park C, Jang SH, Kim CJ, Kim K, et al. High performance organic photosensitizers for dye-sensitized solar cells. Chem Commun 2010;46:1335–7.
[8] Kim D, Lee JK, Kang SO, Ko J. Molecular engineering of organic dyes containing N-aryl carbazole moiety for solar cell. Tetrahedron 2007;63:1913–22.
[9] Zafer C, Gultekin B, Ozsoy C, Tozlu C, Aydin B, Icli S. Carbazole-based organic dye sensitizers for efficient molecular photovoltaics. Sol Energy Mater Sol Cells 2010;94:655–61.
[10] (a) Tian HN, Yang XC, Cong JY, Chen RK, Teng C, Liu J, et al. Effect of different electron donating groups on the performance of dye-sensitized solar cells. Dyes Pigm 2010;84:62–8;
(b) Wu WJ, Yang JB, Hua JL, Tang J, Zhang L, Long YT, et al. Efficient and stable dye-sensitized solar cells based on phenothiazine sensitizers with thiophene units. J Mater Chem 2010;20:1772–9;
(c) Tsao MH, Wu TY, Wang HP, Sun IW, Su SG, Lin YC, et al. An efficient metal-free sensitizer for dye-sensitized solar cells. Mater Lett 2011;65:583–6.
[11] Hwang S, Lee JH, Park C, Lee H, Kim C, Park C, et al. A highly efficient organic sensitizer for dye-sensitized solar cells. Chem Commun; 2007:4887–9.
[12] Ito S, Zakeeruddin SM, Humphry-Baker R, Liska P, Charvet R, Comte P, et al. High-efficiency organic-dye-sensitized solar cells controlled by nanocrystalline-TiO_2 electrode thickness. Adv Mater 2006;18:1202–5.
[13] Ito S, Miura H, Uchida S, Takata M, Sumioka K, Liska P, et al. High-conversion-efficiency organic dye-sensitized solar cells with a novel indoline dye. Chem Commun; 2008:5194–6.
[14] Wan ZQ, Jia CY, Duan YD, Zhang JQ, Zhou LL, Lin Y, et al. Influence of the antennas in starburst triphenylamine-based organic dye-sensitized solar cells: phenothiazine versus carbazole. RSC Adv, submitted for publication.
[15] Wan ZQ, Jia CY, Zhang JQ, Duan YD, Lin Y, Shi Y. Triphenylamine-based starburst dyes with carbazole and phenothiazine antennas for dye-sensitized solar cells. J Power Sources 2012;199:426–31.
[16] Bonhôte P, Dias AP, Papageorgiou N, Kalyanasunda-ram K, Grätzel M. Hydrophobic, highly conductive ambient-temperature molten salts. Inorg Chem 1996;35:1168–78.
[17] Frisch MJ, Trucks GW, Schlegel HB, Scuseria GE, Robb MA, Cheeseman JR, et al. Gaussian 03, Revision C.02. Wallingford, CT: Gaussian Inc.; 2004.
[18] Liu J, Yang HT, Tan WW, Zhou XW, Lin Y. Photovoltaic performance improvement of dye-sensitized solar cells based on tantalum-doped TiO_2 thin films. Electrochim Acta 2010;56:396–400.
[19] Hagfeldt A, Grätzel M. Light-induced redoxreactions in nanocrystalline systems. Chem Rev 1995;95:49–68.
[20] Thomas KRJ, Hsu Y, Lin JT, Lee K, Ho K, Lai C, et al. 2,3-disubstituted thiophene-based organic dyes for solar cells. Chem Mater 2008;20:1830–40.
[21] Ning ZJ, Zhou YC, Zhang Q, Ma DG, Zhang JJ, Tian H. Bisindolylmaleimide derivatives as non-doped red organic light-emitting materials. J Photochem Photobiol A Chem 2007;192:8–16.
[22] Hagfeldt A, Grätzel M. Molecular photovoltaics. Acc Chem Res 2000;33:269–77.